Mark S. Raleigh[1], Ethan D. Gutmann[2], John T. Van Stan II[3], Sean P. Burns[2,4], Peter D. Blanken[4], and Eric E. Small[5]

[1]College of Earth, Ocean, and Atmospheric Sciences, Oregon State University, Corvallis, OR, USA.

[2]National Center for Atmospheric Research, Boulder, CO, USA.

[3]Department of Biological, Geological, and Environmental Sciences, Cleveland State University, Cleveland, OH, USA.

[4]Department of Geography, University of Colorado, Boulder, CO, USA.

[5]Department of Geological Sciences, University of Colorado, Boulder, CO, USA.

Corresponding author: Mark Raleigh (raleigma@oregonstate.edu)

Submitted to: *Water Resources Research*

Key Points:

- Six years of tree sway data from accelerometers on two conifers revealed changes in sway frequency at sub-daily to seasonal scales
- After accounting for thaw-freeze cycles, changes in tree sway due to snow interception were detected and checked with time-lapse images
- Sway data yielded canopy snow mass estimates consistent with snowfall data and storm conditions

Key Words:

snow interception; tree sway; coniferous forests; accelerometers; time-lapse imagery

Index Terms: 0736, 0794, 1985, 1863, 3354

Abstract

Snowpack accumulation in forested watersheds depends on the amount of snow intercepted in the canopy and its partitioning into sublimation, unloading, and melt. A lack of canopy snow measurements limits our ability to evaluate models that simulate canopy processes and predict snowpack and water supply. Here, we tested whether monitoring changes in wind-induced tree sway can enable snow interception detection and estimation of canopy snow water equivalent (SWE). We monitored hourly tree sway across six years based on 12 Hz accelerometer observations on two subalpine conifer trees in Colorado. We developed an approach to distinguish changes in sway frequency due to thermal effects on tree rigidity versus intercepted snow mass. Over 60% of days with canopy snow had a sway signal in the range of possible thermal effects. However, when tree sway decreased outside the range of thermal effects, canopy snow was present 93-95% of the time, as confirmed with classifications of PhenoCam imagery. Using sway tests, we converted significant changes in sway to canopy SWE, which was correlated with total snowstorm amounts from a

nearby SNOTEL site (Spearman r=0.72 to 0.80, p<0.001). Greater canopy SWE was associated with storm temperatures between -7°C and 0°C and wind speeds less than 4 m s^{-1}. Lower canopy SWE prevailed in storms with lower temperatures and higher wind speeds. We conclude that monitoring tree sway is a viable approach for quantifying canopy SWE, but challenges remain in converting changes in sway to mass and further distinguishing thermal and mass effects on tree sway.

1 Introduction

Much of the global seasonal snow zone overlaps forests, which modify hydrological processes and water availability (Essery et al., 2009; Rutter et al., 2009). In forests, snowpack accumulation depends on the amount of snowfall intercepted in the canopy, and the fate of that snow (i.e., sublimation, unloading, melt drip). Coniferous canopies may intercept more than 50% of annual snowfall and reduce snow depth by a similar amount (Hedstrom & Pomeroy, 1998; Lv & Pomeroy, 2020; Martin et al., 2013; John W. Pomeroy & Schmidt, 1993; Storck et al., 2002). Increasing forest density influences not only snow accumulation, but also snowmelt processes (Musselman et al., 2008; Varhola et al., 2010), the timing of which is ecologically significant and dependent on climate (Dickerson-Lange et al., 2017; Lundquist et al., 2013). Thus, knowledge of canopy snow processes is important for understanding and predicting the coupling between forests and the snowpack, an enduring interest to watershed management (Church, 1912).

Reliably quantifying canopy snow interception is an outstanding challenge. A variety of techniques have been tested (Friesen et al., 2015; Kinar & Pomeroy, 2015): measuring branch deflection (Schmidt & Pomeroy, 1990), bagging and weighing intercepted snow on branches (Schmidt & Gluns, 1991), weighing whole trees (Hedstrom & Pomeroy, 1998; Montesi et al., 2004; Nakai et al., 1994; J.W. Pomeroy & Dion, 1996; Storck et al., 2002), and measuring trunk compression (Martin et al., 2013; Van Stan et al., 2013). Although viable, these methods are not commonly used due to substantial environmental disturbances, significant costs, or success in only certain climates (c.f., Gutmann et al., 2017; Martin et al., 2013). Measuring snowfall differences between adjacent forests and open areas can yield indirect estimates of interception (Moeser et al., 2016; Roth & Nolin, 2019) but other processes complicate that approach.

Improved methods for monitoring canopy precipitation storage are needed to improve understanding and prediction of forest hydrological processes (Friesen et al., 2015) and interactions between canopy and the critical zone (Guswa et al., 2020). A low-cost and minimally disruptive approach that can be applied across climates would provide new opportunities to describe dynamics in canopy snow storage and advance model development. Improved descriptions of canopy snow storage dynamics across sites are important to our efforts to mitigate climate change impacts, as most model representations of snow interception are attributed to two field studies (Hedstrom & Pomeroy, 1998; Storck et al., 2002) which diverge when estimating snow interception capacity with warming temperature (Lundquist et al., 2021). Representation of interception and unloading

is a main factor leading to snow model divergence in forested areas (Rutter et al., 2009). The field data needed to evaluate modeled snow interception directly is non-existent in nearly all studies.

Monitoring changes to the natural sway frequency of a tree is a low-cost, non-intrusive, and underexplored approach for quantifying canopy snow mass. Tree sway can be measured with several sensors, such as accelerometers (Hassinen et al., 1998; Yang et al., 2021). Based on mechanical theory (Figure 1), tree sway frequency varies with: (1) changes in mass (e.g., snow interception), and (2) changes in rigidity (Bunce et al., 2019; Mayhead, 1973; Moore & Maguire, 2004). Using accelerometers on a spruce tree, Papesch (1984) measured a reduction in tree sway frequency of 30% in a snow interception event, but did not quantify the mass of canopy snow or effects of tree thermal state. Granucci et al. (2013) used clinometers to measure fluctuations in tree sway as trees froze (more rigid) and thawed (less rigid), but excluded periods with canopy snow. Freezing trees (Gutmann et al., 2017; Lindfors et al., 2019) and snowfall are concomitant in cold climates; to our knowledge, no prior study has disentangled these effects on tree sway.

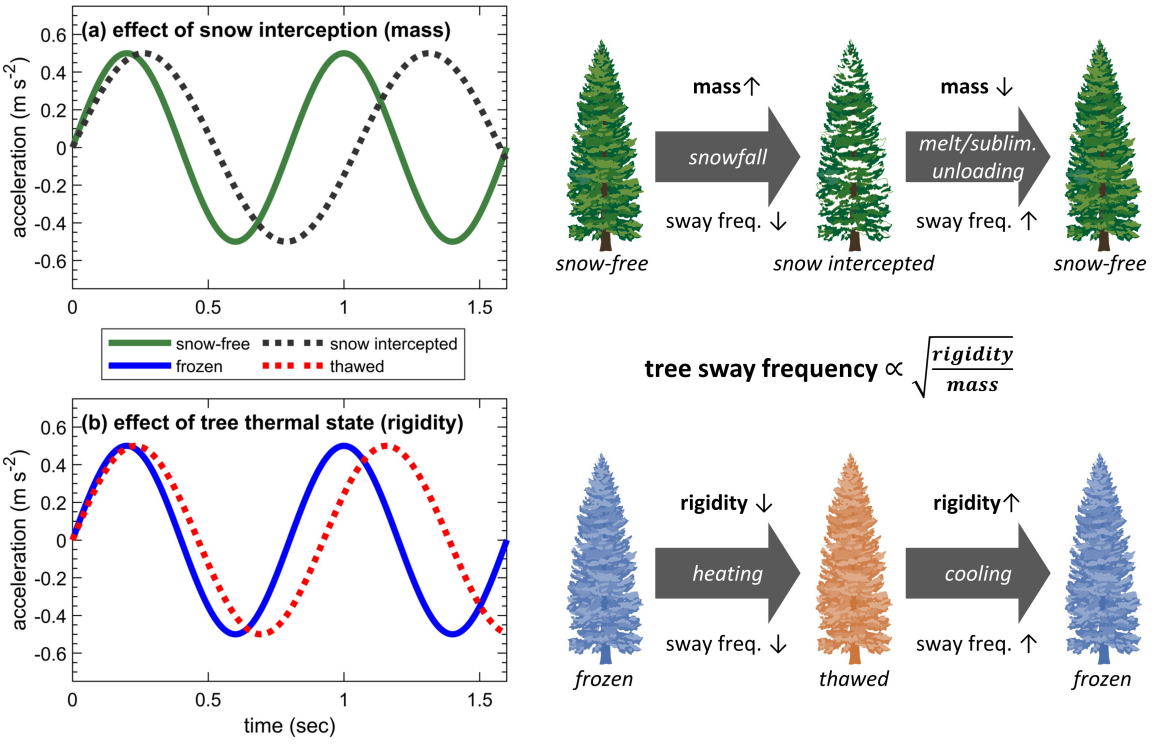

Figure 1. Changes in tree sway frequency with (a) changes in mass due to snow interception and (b) changes in tree rigidity with thermal state (thaw-freeze cycle). The idealized time series (left) show lateral tree acceleration with

wind-induced sway for cases of snow-free vs. snow intercepted and frozen vs. thawed state. Tree sway frequency can decrease as a tree intercepts snow (i.e., added mass) or as a frozen tree thaws (i.e., less rigid).

This "sway-to-mass" measurement concept was proposed to quantify rainfall interception (Friesen et al., 2015; Selker et al., 2011). Sway frequency has been found to decrease with increasing rainfall (van Emmerik et al., 2017). Beyond rainfall interception, tree sway is related to changes in biomass (e.g., tree health, phenology, water content and stress) and biosphere-atmospheric interactions (Baker, 1997; Ciruzzi & Loheide, 2019; van Emmerik et al., 2018; Gougherty et al., 2018; T. D. Jackson et al., 2021; Kooreman, 2013). Most studies have occurred in warmer conditions and have not needed to distinguish between mass and thermal effects on tree sway (Figure 1). Jackson et al. (2021) note "This could be particularly interesting in sites which freeze in winter since this will have a profound effect on the wood elasticity."

The goal of this paper is to assess the feasibility of separating mass and thermal effects on tree sway, and demonstrate the potential for tree sway monitoring to enable quantification of canopy snow interception. We address two questions: (1) Can snow interception events be detected in tree sway time series? (2) How do sway-based estimates of canopy snow mass vary as a function of snowstorm characteristics? In the process, we identify the main challenges for this type of monitoring and highlight potential paths forward for improving this approach.

We monitored wind-induced movement of two trees with accelerometers for six years (2014-2020) in a coniferous forest of the Colorado Rocky Mountains. From these data, we derive hourly tree sway frequency and attempt to isolate tree sway variations due to thermal effects. Changes in tree sway unexplained by thermal effects enable snow interception detection. We also propose and test an empirical method for converting changes in sway to canopy snow mass.

2 Study Site, Sensors, and Data

2.1 Study sites and tree characteristics

We monitored tree sway from November 2014 – August 2020 in a subalpine coniferous forest near the Niwot Ridge Long-Term Ecological Research (LTER) site in the Colorado Front Range, USA (Figure 2a). The C-1 site (N40.033, W105.547) is located at 3050 m elevation. Above-canopy wind speed averaged 5.2 m s^{-1} during the snow season (October-May), while mid-winter (December-February) air temperature averaged -6.5 °C. This was an ideal study site, given ample winds to activate tree motion, available scientific infrastructure, and prior forest research (e.g., Bowling et al., 2018; Gutmann et al., 2017; Molotch et al., 2007).

We instrumented two trees adjacent to the Niwot Ridge Subalpine Forest (US-NR1) AmeriFlux tower (Figure 2): a *Picea engelmannii* (engelmann spruce) and an *Abies lasiocarpa* (subalpine fir). These trees were selected because they represented two of the dominant species in the forest (Turnipseed et al., 2002),

and because they were accessible from a tower platform next to the canopy edge (Fig. 2c). This platform did not impede tree motion.

The forest in the vicinity of the tower has trees aged in the 100-250 year range (S P Burns, 2018). Tree height is typically around 10-15 m (Fig. 2b), with a mean canopy gap fraction of 17% and a leaf area index of 3.8 to 4.2 m^2 m^{-2} (Turnipseed et al., 2002). The study trees were in close proximity to each other but not close enough for crown collisions (Fig. 2c). Tree height was 13.0 m for the spruce and 11.0 m for the fir. Diameter at breast height (DBH) was 35.7 cm for the spruce and 18.5 cm for the fir. Based on the average of multiple radial measurements from canopy edge to bole, the effective crown diameter (D_c) was 3.4 m for the spruce and 1.7 m for the fir.

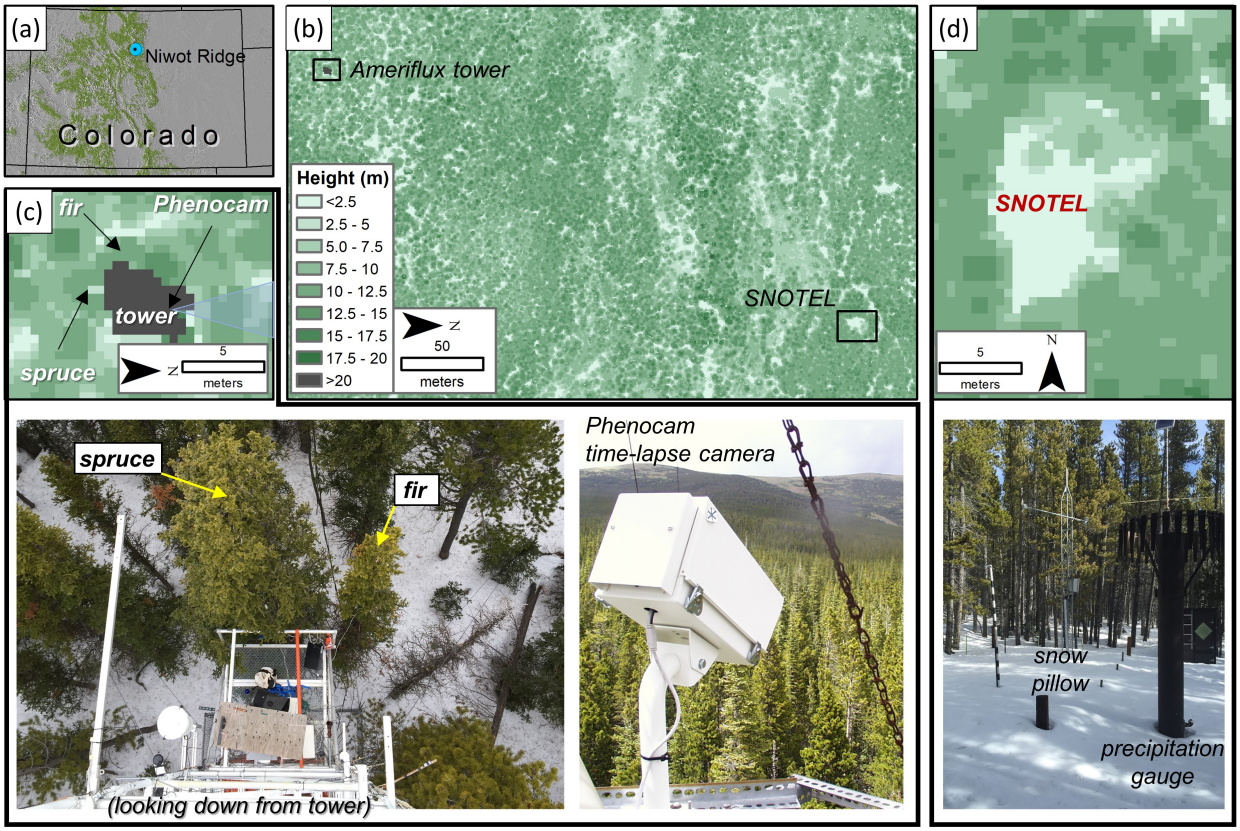

Figure 2. Study site maps and photos. (a) Map of Niwot Ridge in Colorado, with green regions mapping forests. (b) Tree height map showing locations of the AmeriFlux tower and SNOTEL site in a forest gap, with (c-d) zoomed maps and photos. Tree height maps are derived from an airborne lidar survey (Harpold et al., 2014) and gridded at 0.5 m resolution. Note north is to the right in (b) and (c) but up in (d).

2.2. Accelerometers and acceleration measurements

On each tree bole, we installed a single three-axis accelerometer to record acceleration associated with wind-induced tree movement (Figure 3). Installation heights were 8.9 m on the spruce and 8.1 m on the fir. Both accelerometers were Gulf Coast Data Concepts (GCDC) model X16-1D. Evans et al. (2014) compared multiple accelerometers and found GCDC had minimal noise but an uneven sampling rate. Therefore, we processed acceleration data using a frequency analysis for unevenly-sampled data (section 3.2). Prior to installation, we conducted a three-axis tumble test where the sensors were systematically rotated to ensure each axis recorded gravity when oriented downward. An installed USB extension cable provided external power to the sensor, enabled data download, and permitted sensor programming at an access port without disturbing the sensor (Figure 3). Each accelerometer logged three-axis acceleration data at ~12 Hz nearly continuously over the study, yielding an 83 GB data volume total for both trees (Raleigh, 2021b, 2021a). Total cost of materials was about $125 USD per installation. Further details are in Text S1.

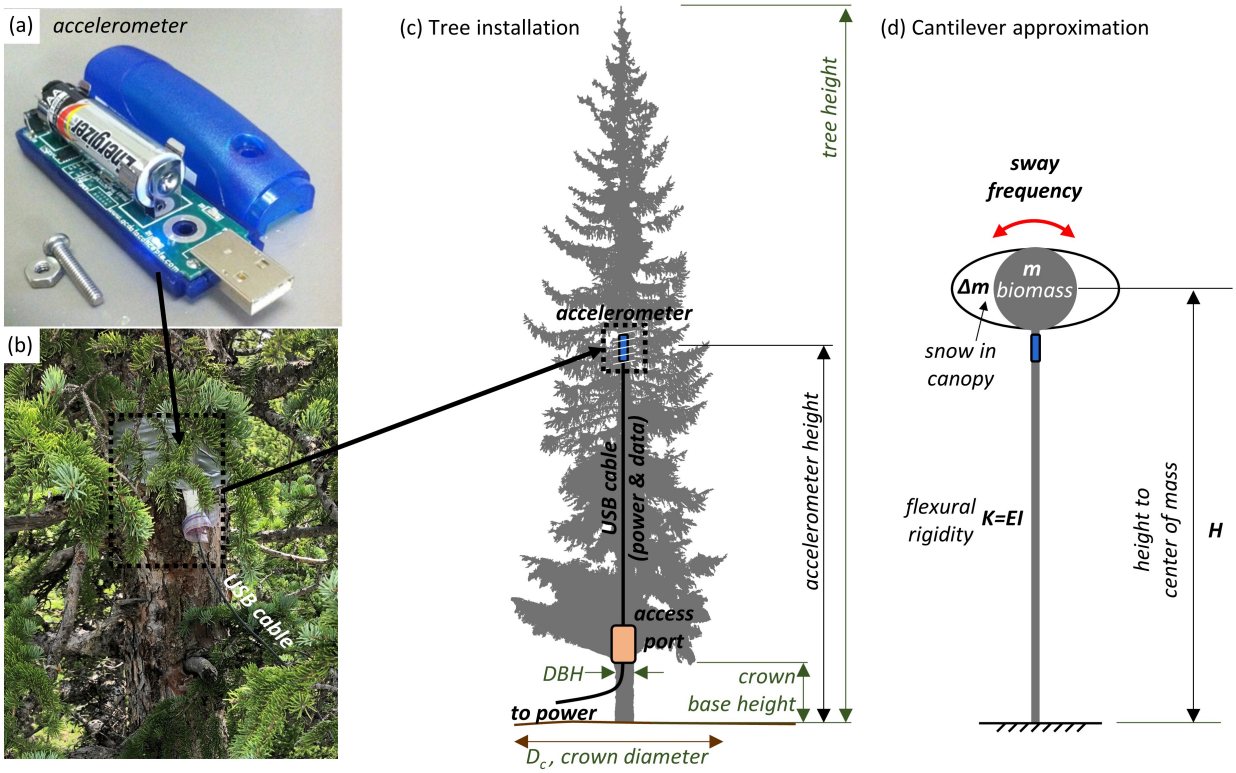

Figure 3. (a) GCDC accelerometer with cover removed. (b) Accelerometer installation on the spruce bole. (c) Conceptual installation and measurements. (d) Approximation of the tree as a cantilever with biomass (m), a transient snow load (Δm), and tree flexural rigidity (K) defined by modulus of elasticity (E)

and area moment of inertia (I).

2.3. Time-lapse imagery and canopy snow classification

A time-lapse camera enabled independent documentation of snow interception (Fig. 2c). Camera images were acquired from the PhenoCam network (Richardson et al., 2018), specifically camera "niwot2" before July 2015 and camera "niwot3" after July 2015. The camera models were StarDot NetCam XL for niwot2 and StarDot NetCam SC for niwot3. Although the cameras pointed away from the study trees (Fig. 2c), snow loading and unloading was consistent on trees around the tower, based on independent field and camera observations (no data shown).

We manually classified daily canopy snow presence by examining up to four PhenoCam images per day (8 AM, 11 AM, 2 PM, 5 PM); if any of those images showed canopy snow, that day was recorded as having snow interception. While many images were unambiguous in the classification, there were cases with modest amounts of canopy snow (e.g., light dusting of snow or sporadic clumps persisting in time); we recorded these as snow interception days. In separate analyses (not shown) we tested automated classifiers (i.e., machine learning, pixel thresholding) but these were inconsistent relative to manual classifications.

2.4. Meteorology, tree temperature, and snowfall data

The study trees were located next to the US-NR1 AmeriFlux tower (Fig. 2c), which included measurements of the local meteorological conditions (S. P. Burns et al., 2015). We used wind speed (Campbell Scientific CSAT3 Sonic anemometer, 21 m height), relative humidity and air temperature (Vaisala HMP-35D, 8 m height), and atmospheric pressure (Vaisala PTB-101B, 12 m height) to characterize storm conditions (see Text S2).

To isolate thermal effects on tree sway, we modeled tree sway as a function of temperature (section 3.3) based on local tree bole temperatures (S. P. Burns et al., 2015; Turnipseed et al., 2002). Bole temperatures were collected with Campbell A3537 (T-type Thermocouples) sensors at 2 cm depth. Bole temperature data were missing prior to fall 2015, and were thus unavailable in the first study year. For periods when bole temperatures were unavailable, we substituted smoothed air temperature as a proxy (Lindfors et al., 2019), which lags bole temperatures (Bowling et al., 2018; Sean P. Burns et al., 2018; Silins et al., 2000). Both bole and air temperature were aggregated from 30-min to hourly values using a cubic smoothing spline ("fit.m" in Matlab). Air temperatures were further smoothed with a 36-hour moving average window, which yielded similar variance as winter bole temperatures.

The study area included a nearby NRCS SNOw TELemetry (SNOTEL) station, located in a ~10 m forest gap 360 m northeast and 20 m below the study site (Fig. 2b,d). We used hourly SNOTEL snow water equivalent (SWE) data to assess the snowstorm magnitudes, for comparison to the sway-to-mass approach. We quality controlled and filtered hourly SWE data and then took all

positive increments of hourly SWE as snowfall amounts. For each storm, the total snowfall was determined as the sum of all hourly snowfall from the start to end of the interception event, as detected in the sway data. We checked the snowfall derived from the SNOTEL SWE against data from two nearby precipitation gauges (1) at the same SNOTEL site (Fig. 2d) and (2) at the "Hills Mill" U.S. Climate Reference Network (USCRN) site, located in a more exposed area outside the forest 400 m to the east and 30 m below the study site. Winter SNOTEL precipitation was typically within 5% of SWE-derived snowfall amounts, while the USCRN data typically had 40% less winter precipitation than both SNOTEL datasets. We therefore used hourly snowfall derived from SNOTEL SWE to quantify storm totals.

3 Theory and Methods

3.1. Mechanical theory

When subject to a wind gust, a coniferous tree sways in a manner characteristic of a damped harmonic oscillator, e.g., a vertical cantilever beam (Fig. 3d) (Blevins, 1979; Bunce et al., 2019; Dargahi et al., 2020; Gardiner, 1992; T. Jackson et al., 2019; Moore & Maguire, 2004; Peltola, 1996; Pivato et al., 2014). In this approximation, the natural sway frequency (f, Hz) depends on its mechanical, geometric, and mass properties:

$$f \propto \frac{1}{2\pi}\sqrt{\frac{K}{m}} \quad (1)$$

where K is the flexural rigidity (or stiffness) and m is the total mass of the tree, including biomass and canopy water storage. Sway frequency (f) in Equation 1 is independent of wind speed, as long as there is sufficient wind to activate tree motion (see Text S2 and Figure S5). A tree may have multiple natural sway frequencies, but the first natural frequency dominates the sway response of a tree (Moore & Maguire, 2004) and is thus our focus.

In Equation 1, rigidity is the product of Young's modulus of elasticity (E; mechanical property) and the area moment of inertia (I, geometric property); K=EI. E is a measure of resistance to elastic deformation per unit stress; a higher value signifies a more rigid tree. I depends on the cross-sectional geometry of the tree and is inversely related to tree diameter. E data for standing trees are scarce (Friesen et al., 2015) and were not measured here. Green wood E values are available in handbooks (USDA Forest Service, 2010) with nominal values of 7100-8600 MPa for engelmann spruce and 7200-8700 MPa for subalpine fir. However, our approach did not require an estimate of E, as we empirically related changes in f to changes in m while accounting for temperature effects on K (see sections 3.3-3.4).

Both components of tree rigidity (E and I) vary with temperature and moisture content, especially in transitions between freezing and thawing states (Charrier et al., 2014, 2017; Gao et al., 2015; Gerhards, 1982; Green & Evans, 2008; Onwona-Agyeman et al., 1995; Sun et al., 2019). When temperatures are below the freezing point, the xylem of trees can freeze (e.g., Bowling et al., 2018;

Charrier et al., 2014, 2017; Gutmann et al., 2017). Freezing of tree xylem results in two opposing effects: (1) an increase in E (Gerhards, 1982; Green et al., 1999; Green & Evans, 2008; Lindfors et al., 2019; Silins et al., 2000), and (2) a decrease in I due to a shrinkage in tree diameter (Charrier et al., 2017; Lindfors et al., 2019). Observational studies show that tree sway frequency increases under freezing conditions relative to thawed conditions (Granucci et al., 2013), suggesting that the increase in E dominates the thermal effect on tree sway.

3.2. Frequency analysis of acceleration data

To obtain hourly time series of observed tree sway frequency (f_{obs}), we conducted frequency analyses on the 12 Hz data from the two lateral axes (N-S and E-W) of the accelerometers (section 2.2). We excluded the vertical axis data which were less sensitive to tree motion and had less consistent sway information. Data processing included three main steps: (1) frequency analysis, (2) filtering, and (3) smoothing.

Step 1. Frequency analysis was conducted on each lateral axis using a non-overlapping sliding window of 1 hour, such that ~45000 acceleration data were analyzed to identify one sway frequency value each hour. This window was short enough to resolve snow interception events while reducing noise relative to a shorter window (Text S3, Figures S7-S8). We used the Lomb-Scargle Periodogram (Lomb 1976; Scargle 1982), which yields Fourier-like estimates of power spectral density (PSD) for an unevenly sampled signal (section 2.2). In each window, we detrended the acceleration data, and then implemented the Lomb-Scargle analysis using Matlab (function "plomb.m"), with an oversampling factor of 2 and a maximum frequency of 3 Hz. The hourly tree sway frequency (Hz) was the frequency value with maximum PSD. We did not analyze other metrics such as frequency spectrum slope (van Emmerik et al., 2017).

Step 2. Hourly frequency data were filtered by removing any data that did not meet a minimum power level threshold of 0.99 (i.e., probability test of a true signal) and any outliers (i.e., 3 standard deviations) relative to the mean sway frequency in a sliding 72-hour window.

Step 3. To fill gaps in the time series, we smoothed sway frequency using splines with a smoothing parameter of 0.99. Smoothed sway frequency was highly correlated between axes (r=0.93 for spruce axes, r=0.98 for fir axes, not shown). Therefore, for each tree, we averaged the hourly smoothed sway frequency between the lateral axes for use in subsequent analyses.

Data processing for a 12-day example is illustrated in Figure 4. This shows that variations in tree motion scale with wind speed (Fig. 4a and Figure S6), but tree sway frequency does not vary with wind speed (Fig. 4e and Figure S5). In this 12-day interval, tree sway frequency was reduced on 22 December and 28 December, relative to ambient values. These occurred due to transient changes in either mass (e.g., snow interception) or tree rigidity (e.g., tree thaw).

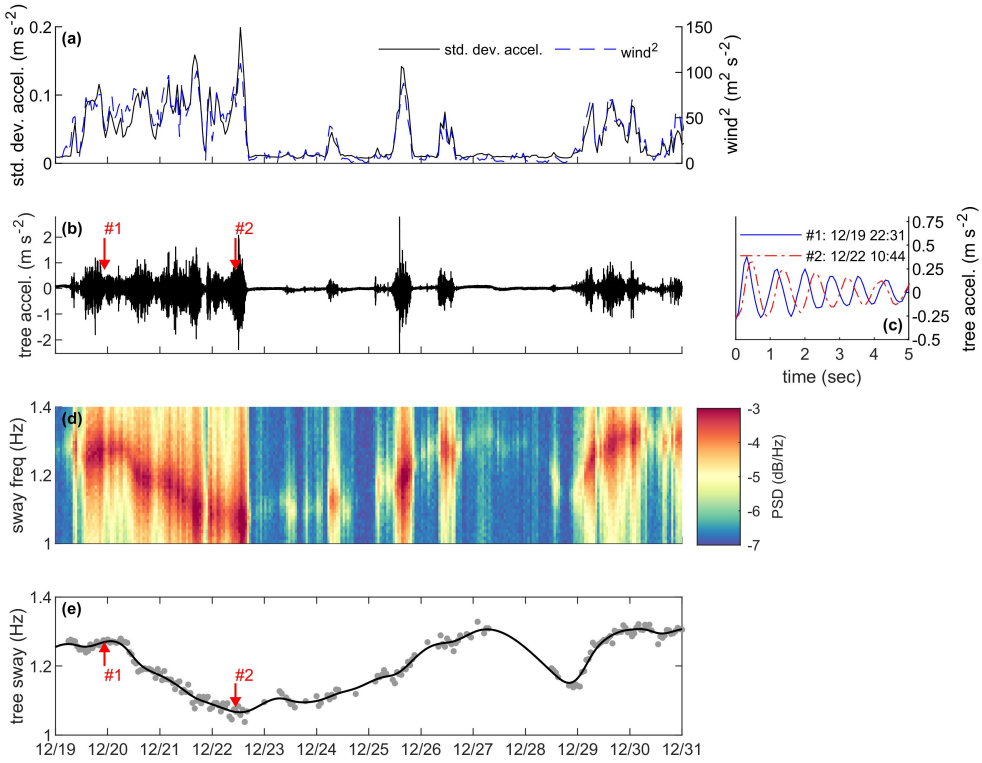

Figure 4. Example of measured and processed data for the east-west axis on the spruce tree in late December 2019. (a) Squared wind speed and hourly standard deviation in tree acceleration, showing tree motion scaling with wind energy. Measured 12 Hz tree acceleration over (b) the 12 day interval and (c) zoomed into two example sway events displayed over a 5 second interval. Event #2 had fewer sway cycles (~5.5 cycles) than event #1 (~6.5 cycles). (d) Hourly Lomb-Scargle power spectral density (PSD) displayed as a spectrogram, which shows the strength of frequencies in each hourly window. (e) Hourly tree sway, taken as the frequency with the maximum PSD in each hourly window (gray circles), and then filtered and smoothed to fill gaps (black line). Tree sway decreased from 1.27 Hz in event #1 to 1.08 Hz in event #2.

3.3. Distinguishing changes in sway frequency: thermal vs. mass effects

We assumed temporal changes in coniferous tree sway through the snow season (October-May) were due to either (1) gains/losses of water mass (i.e., snow) in the canopy, or (2) changes in rigidity due to thermal state (Figure 1) or a combination thereof. Thus, we hypothesized that controlling for changes in rigidity would reveal the incidence and magnitude of snow interception. We neglected

other factors that can influence tree sway, such as changes in moisture content (likely more important in the growing season) and variations in the vertical center of mass due to uneven snow loading and unloading (see discussion). Changes in sway due to annual tree growth were accounted for implicitly by analyzing each year separately.

We assumed observed sway frequency (f_{obs}) had two components: (1) an unloaded sway frequency (f_0) that varied only with temperature and assumed a snow-free canopy, and (2) intermittent changes in sway (Δf) which were due to snow interception:

$$f_{\text{obs}} = f_0(T) - f \quad (2)$$

Therefore, in snow-free periods, Δf=0, and thus $f_{obs} = f_0$. In periods with snow interception, we expected positive differences between f_0 and f_{obs}:

$$f = f_0(T) - f_{\text{obs}} \quad (3)$$

Computing Equation 3 required a dynamic estimate of the unloaded sway frequency with temperature. We assumed this temperature-dependency was driven by changes in E, which increases as temperature decreases, with a sharper transition near the freezing point, and more modest changes at higher (>5°C) and lower (<-5°C) temperatures (Bowling et al., 2018; Gao et al., 2013, 2015; Green & Evans, 2008; Schmidt & Pomeroy, 1990; Silins et al., 2000; Sun et al., 2019). We represented this relationship as a sloped sigmoidal curve:

$$f_0(T) = \frac{a-c}{1+e^{(-Tb-d)}} + c - hT \quad (4)$$

where a is a characteristic sway frequency (Hz) when frozen, b is a scaling parameter (°C^{-1}) controlling the slope through the freeze-thaw zone, c is a characteristic sway frequency (Hz) when thawed, d is a shifting parameter accounting for temperature bias, T is temperature (air temperature, T_a, for WY 2015 and bole temperature, T_b for WY 2016-2020), and h is a slope parameter that permits sway to decrease linearly with T outside the freeze-thaw zone.

We fit and evaluated Equation 4 separately for each tree and year (Text S4). In each year, we randomly selected training points (n=1000 hours) when the PhenoCam imagery showed snow-free canopy, and fit Equation 4 to the hourly observed sway (f_{obs}) data. We used bole temperatures in water years (WY) 2016-2020, and 36-hour air temperatures in WY 2015 (when bole temperatures were unavailable), and compared the fit statistics when both temperature datasets were available (Text S4, Figures S9-S10, Tables S2-S3).

When f_{obs} decreased significantly below f_0 (i.e., outside the range of thermal effects), we assumed snow was in the canopy and mass effects drove the decrease in tree sway. Detection of these events was achieved with the signal-to-noise ratio (SNR), a common metric for identifying meaningful information in a signal. SNR was calculated as Δf divided by the standard deviation of errors between estimated (f_0) and observed sway (f_{obs}) using the training points (see above). Standard deviation in sway error varied with both T_b and T_a, with the lowest

variations at the lowest temperatures and the highest variations in error near T_b=3°C for the fir and T_b=4°C for the spruce (Figure S11); thus, SNR was temperature-dependent. For cases with Δf >0, we identified snow interception when SNR 3, which corresponds to a 1% probability of a false positive, assuming a normal distribution. When SNR<3 or Δf <0, we assumed thermal effects and mass effects cannot be distinguished in the sway data without independent information.

3.4. Evaluation of detected canopy snow

Applying the above thresholds for SNR and Δf yielded a sway-based estimate of when canopy snow was present. We evaluated this detection of canopy snow presence against PhenoCam imagery over the six snow seasons (1 October – 31 May). For this evaluation, we excluded the training points used to fit Equation 4, which enabled an independent assessment of canopy snow detection. We first aggregated the sway-based classifications of canopy snow (1=present, 0=absent) to daily values. We then computed standard commission and omission metrics of precision and recall, similar to snow mapping studies (e.g., Lv & Pomeroy, 2019; Raleigh et al., 2013):

$$Precision = \frac{\mathrm{TP}}{TP+FP} \quad (5)$$

$$Recall = \frac{\mathrm{TP}}{TP+FN} \quad (6)$$

where true positives (TP) had canopy snow in both datasets, false positives (FP) had canopy snow in the sway data only, and false negatives (FN) had canopy snow in the imagery only. Precision computed the fraction of days when canopy snow detected by sway was confirmed with the imagery. Recall computed the fraction of all days with canopy snow that were detected in the sway data.

3.5. Estimating canopy SWE from decreases in tree sway frequency

We estimated canopy SWE from Δf after SNR filtering (section 3.3). To convert Δf to a change in mass (Δm), we conducted multiple sway tests at each tree to empirically define the relationship. In these tests (Fig. 5a), we induced sway by pulling on the unloaded tree (Δm=0) with a rope and suddenly releasing it (Mayhead, 1973) to produce swaying motion in both lateral directions. The accelerometer recorded acceleration while each tree was freely swaying (Fig. 5b), enabling identification of unloaded sway frequency (f_0). We then conducted a series of tests where we attached a known mass (Δm) to the bole, induced sway again, and recorded Δf relative to the first test with no mass in the canopy (Fig. 5b). We conducted tests with a range of masses up to 61 kg; heavier masses raised logistical and safety concerns. For a given Δm, we induced sway at least five times, and found the sway frequency across all trials.

Sway tests occurred under thawed conditions on four dates on both trees (September 2015, December 2015, June 2016, October 2017), with a fifth test on the fir tree (February 2016). Conducting tests under freezing conditions were too challenging. For each tree and test, the mass was placed at approximately

the same height (i.e., ~7.5 m).

We fit a linear relationship (zero intercept) to the Δf and Δm data from the sway tests:

$$m = \alpha \times f \quad (7)$$

where is a slope parameter (kg Hz^{-1}) that specifies that scaling of mass with a change in sway frequency. To characterize uncertainty, we computed 95% confidence intervals (C.I.) on to account for measurement errors in Δm and Δf. The data and fit are shown in Figure 5c with more information in Text S5 and Table S4. The spruce had a steeper slope than the fir, presumably due to greater biomass. We were unable to test how the slope might change with temperature and thermal changes in tree rigidity; see discussion for potential effects of this assumption.

Finally, we converted Δm to canopy SWE (mm) per unit area based on the vertical projected tree area (based on crown diameter D_c, Section 2.1), following Storck et al. (2002):

$$\mathrm{SWE_{can}} = \frac{4\Delta m}{\pi D_c^2} \quad (8)$$

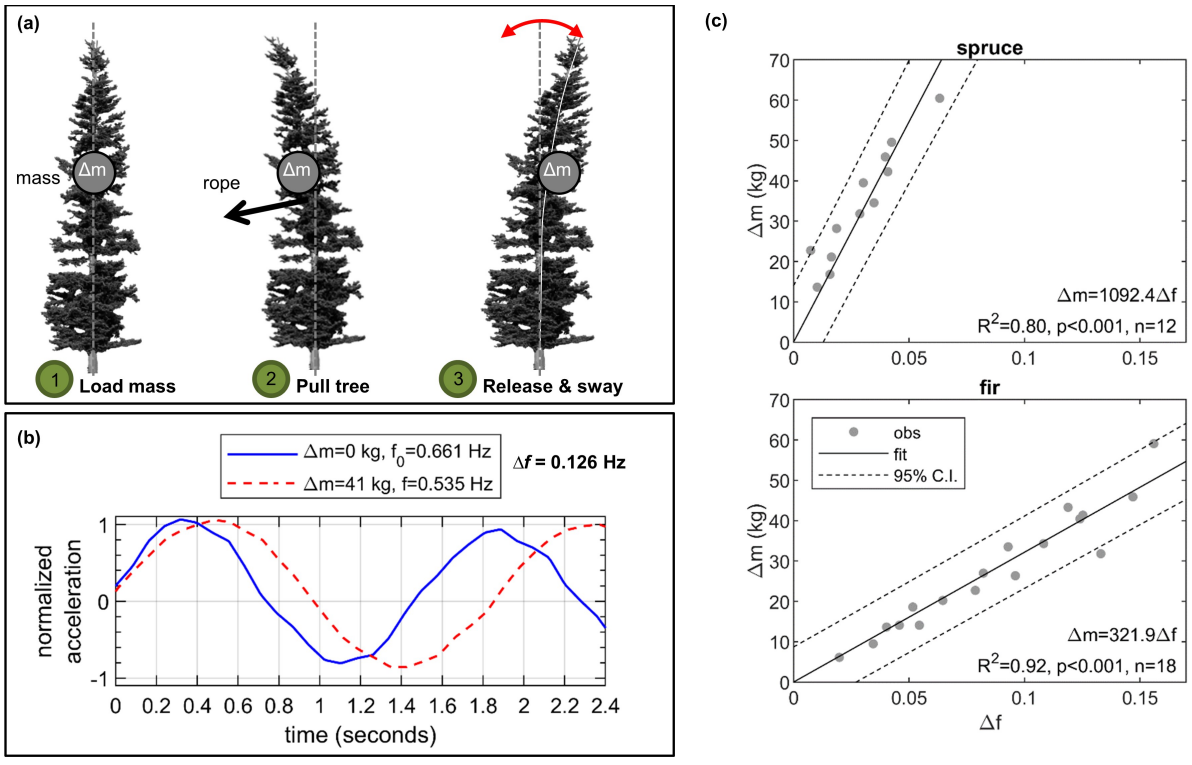

Figure 5. (a) Tree sway test, where a known mass (Δm) was fixed to the bole, the tree was pulled and released to induce sway. (b) Tree acceleration data

(normalized) for two tests, including no added mass (blue line) and an added mass of 41 kg, which decreased sway by 0.126 Hz. (c) Derived relationships between decrease in sway (Δf) and added mass (Δm) for all tests conducted on the spruce and fir trees.

4 Results

4.1. Tree sway variations

Time series of hourly tree sway were derived from the observed acceleration data on the spruce and fir trees over 2014-2020. Tree sway was significantly correlated between the two trees (Pearson correlation r=0.92, Figure 6). Tree sway varied seasonally, with higher frequency during winter and lower frequency during summer, with variations coinciding with temperature rather than wind speed (Text S2, Fig S5). Sway frequency declined until mid-summer and then increased through fall. Sporadic decreases in sway frequency were evident throughout the year, but were larger and more common in the snow season (October-May) than in the warm season (June-September). Decreases in sway frequency during summer were not analyzed but often coincided with rainfall (not shown). Over the six years, mean sway frequency increased from 1.05 to 1.07 Hz for the spruce (2% increase) and from 0.65 to 0.73 Hz for the fir (12% increase).

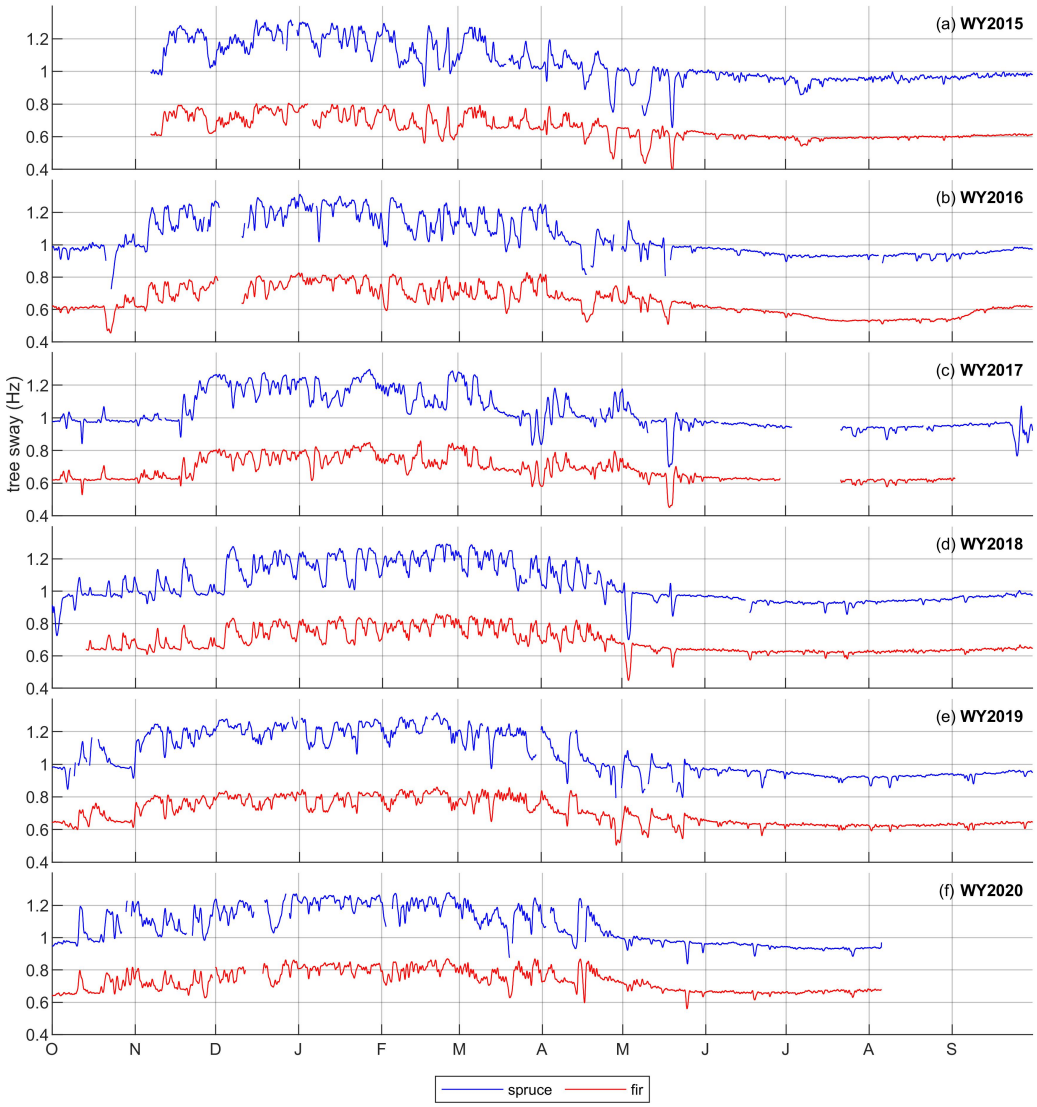

Figure 6. Observed hourly tree sway (Hz) derived from accelerometer data recorded on spruce and fir trees from water years 2015-2020 (a-f). Data gaps exceeding 1 day are omitted.

4.2. Distinguishing sway changes between thermal effects and snow interception

The modeled relationship between temperature and unloaded sway frequency (f_0) was evaluated (see Tables S2-S3). The R^2 ranged from 0.89-0.95 for the spruce and 0.71-0.87 for the fir, with root mean squared error (RMSE) ranging

from 0.02-0.03 Hz for both trees. The standard deviation in f_0 residuals (for SNR calculations) varied with temperature, with the lowest value of 0.02 Hz at -10 °C for both trees, and the highest of 0.13 Hz (spruce) and 0.09 Hz (fir) around 3 to 4 °C. Analysis showed similar statistical fit for air and bole temperatures (see Text S4), supported the use of air temperature when bole temperatures were unavailable (i.e., WY 2015).

Comparing f_0 to observed sway (f_{obs}) allowed us to isolate when sway frequency was varying due to thermal effects. To illustrate, we highlight water year 2017 in Figure 7. Over many intervals, f_{obs} tracked f_0 (Fig. 7a), which suggested thermal effects drove those variations (e.g., sway decrease in mid-February). However, there were also multiple intervals when f_{obs} diverged from f_0 (e.g., three events near 1 April, one large event in mid-May). These often coincided with times when canopy snow was identified in the imagery (gray zones, Figure 7).

We computed Δf (Equation 3) by subtracting f_{obs} from $f_{0,}$ which clarified the magnitude and timing of decreases in sway frequency unexplained by thermal effects (Fig. 7b). Intervals when the Δf SNR 3 (highlighted in blue) were all coincident with times when the camera classification showed snow in the canopy. The magnitude of Δf varied seasonally, with higher Δf in the late fall and spring (e.g., May 2017), and more modest Δf in cold winter months (e.g., January 2017). Some events with positive Δf did not meet the SNR 3 requirement for canopy snow detection; mass and thermal effects could not be distinguished in those cases (e.g., 7-8 February). Note that in some periods the duration of canopy snow were overemphasized in the image analysis (e.g., most of January 2017) due to persistent, isolated clumps of canopy snow.

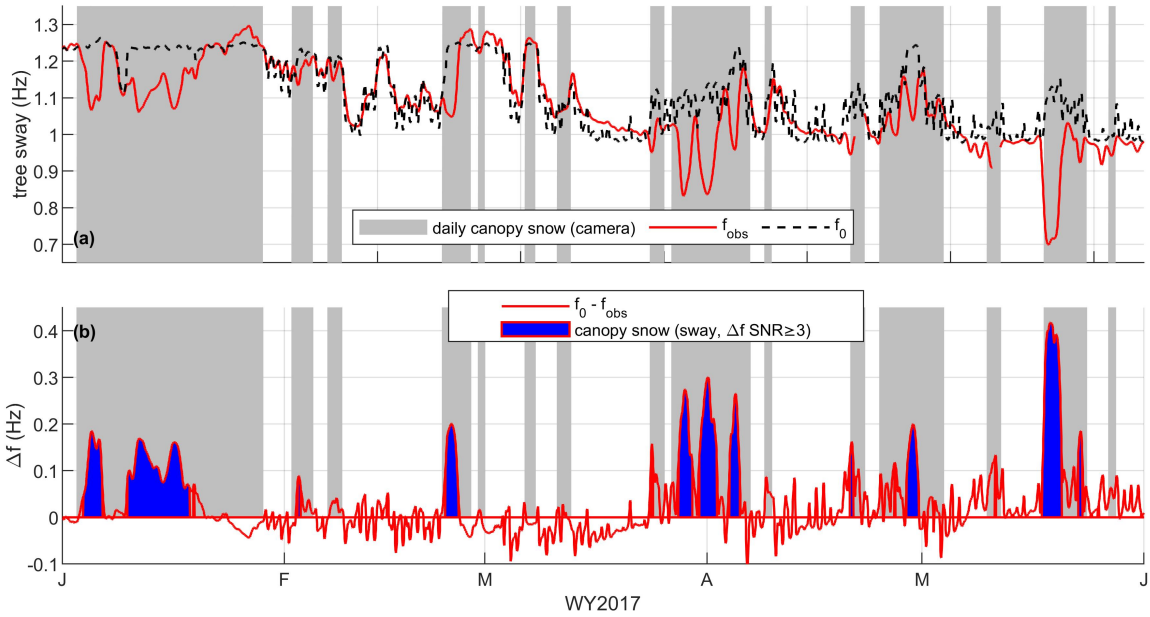

Figure 7. (a) Hourly observed tree sway (f_{obs}) and unloaded tree sway (f_0) estimated from bole temperature and Equation 4. (b) Changes in sway frequency (i.e., differences between f_0 and f_{obs}, Equation 3). Gray areas are intervals when daily classifications of time-lapse camera imagery showed snow in the canopy. The blue intervals are events when Δf SNR 3 and thus canopy snow is detected in the sway data. Example is from the spruce tree during water year 2017.

We assessed the detectability of canopy snow in the sway data. The distribution of Δf based on canopy snow presence or absence showed broad overlap at low values of Δf, typically less than 0.1 Hz (blue vs. green in Figure 8). However, larger values of Δf typically coincided with canopy snow. When constraining to intervals when the SNR 3 threshold was enforced for canopy snow detection, distributions were more distinct (compare red vs. green in Figure 8). The precision metric for canopy snow detection (with SNR 3) was 0.93 for the spruce and 0.95 for the fir, indicating that most days with canopy snow detected in the sway data were corroborated with image analysis. In contrast, the recall metric was 0.40 for the spruce and 0.36 for the fir, indicating that 60-64% of days with canopy snow (known from the imagery) were not detected in the sway data. The low recall was influenced by several intervals when the mass of canopy snow was minimal (e.g., dusting of snow in canopy or isolated snow clumps). Recall can be improved using a lower SNR threshold, but with a tradeoff of reduced precision (not shown).

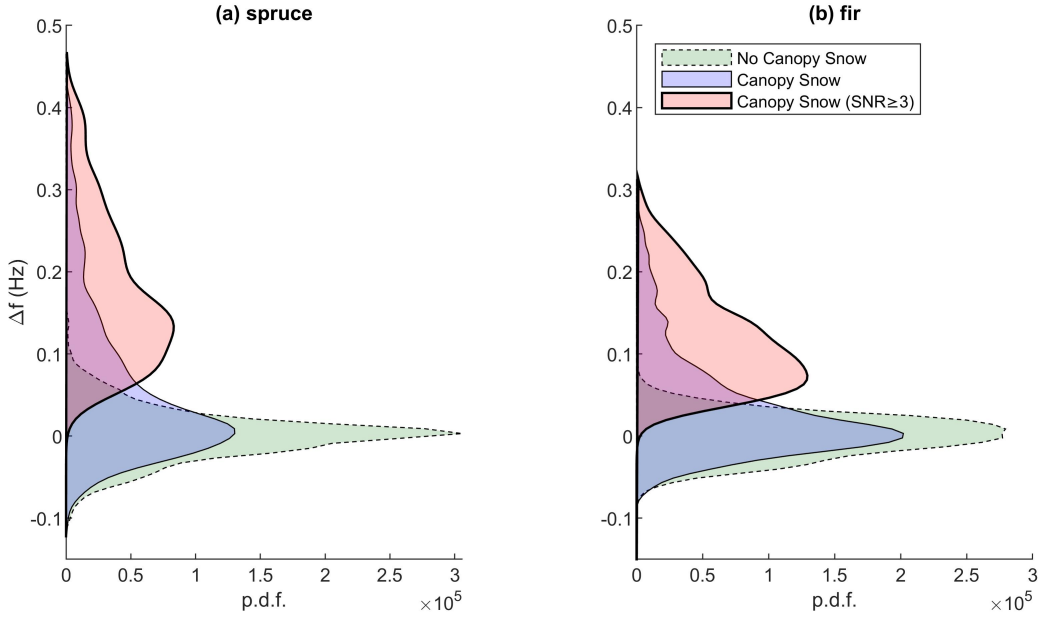

Figure 8. Probability distribution functions (pdfs) of Δf for the (a) spruce and (b) fir, with different distributions shown for intervals when canopy snow was absent or present, based on daily time-lapse camera classification. The canopy snow pdfs are separated for all points (blue) and only points exceeding the SNR detection limit (red).

4.3. Estimating canopy SWE and contextualizing with snowstorm attributes

We next examined canopy SWE estimated from changes in tree sway frequency and compared those estimates to snowstorm magnitudes and characteristics (Figure 9). With the data, we identified and analyzed 137 snow interception events in the spruce data and 136 events in the fir data over the six year period, confirmed in both the tree sway data (Δf >0 and SNR 3) and PhenoCam images. The interception events analyzed for these neighboring trees were slightly different due to tree-to-tree differences in SNR. For each storm, we calculated the total snowfall (section 2.4), and mean wet bulb temperature, and mean wind speed. Changes in sway were converted to canopy SWE following Equations 7 and 8.

Both trees showed a general increase in canopy SWE with increasing storm totals (Fig. 9a,d). Based on Spearman's ranked correlation between canopy SWE and storm totals, we calculated r=0.72 for the spruce and r=0.80 for the fir with p<0.001 for both trees. Images from four example storms (s1-s4) also qualitatively supported the general increase in canopy SWE with storm total (Figure 9). A wide range of storm totals produced a similar canopy SWE. For example, the 10 highest canopy SWE amounts (44-56 mm for the spruce, and 32-

44 mm for the fir) coincided with storms ranging from 10 to 72 mm of snowfall (Fig. 9a,c). Note that many canopy SWE values exceeded the storm total (left of 1:1 line), suggesting a high bias in the sway-to-mass data, a low bias in the SNOTEL data or both. One of the largest interception events was in mid-May 2017, which was a 70 mm snowstorm that registered canopy SWE of 50 mm on the spruce and 44 mm on the fir (s4 in Figure 9). Lower canopy SWE values ($<$ 20 mm for both trees) were generally confined to storm totals less than 25 mm SWE.

Across storms, canopy SWE had significant but modest correlations with temperatures (Fig. 9b,e) and wind speeds (Fig. 9c,f). For both trees, the highest canopy SWE values were associated with temperatures between -7°C and 0°C and wind speeds less than 4 m s^{-1}. Lower canopy SWE values were found in storms with lower temperature storms and high wind speeds.

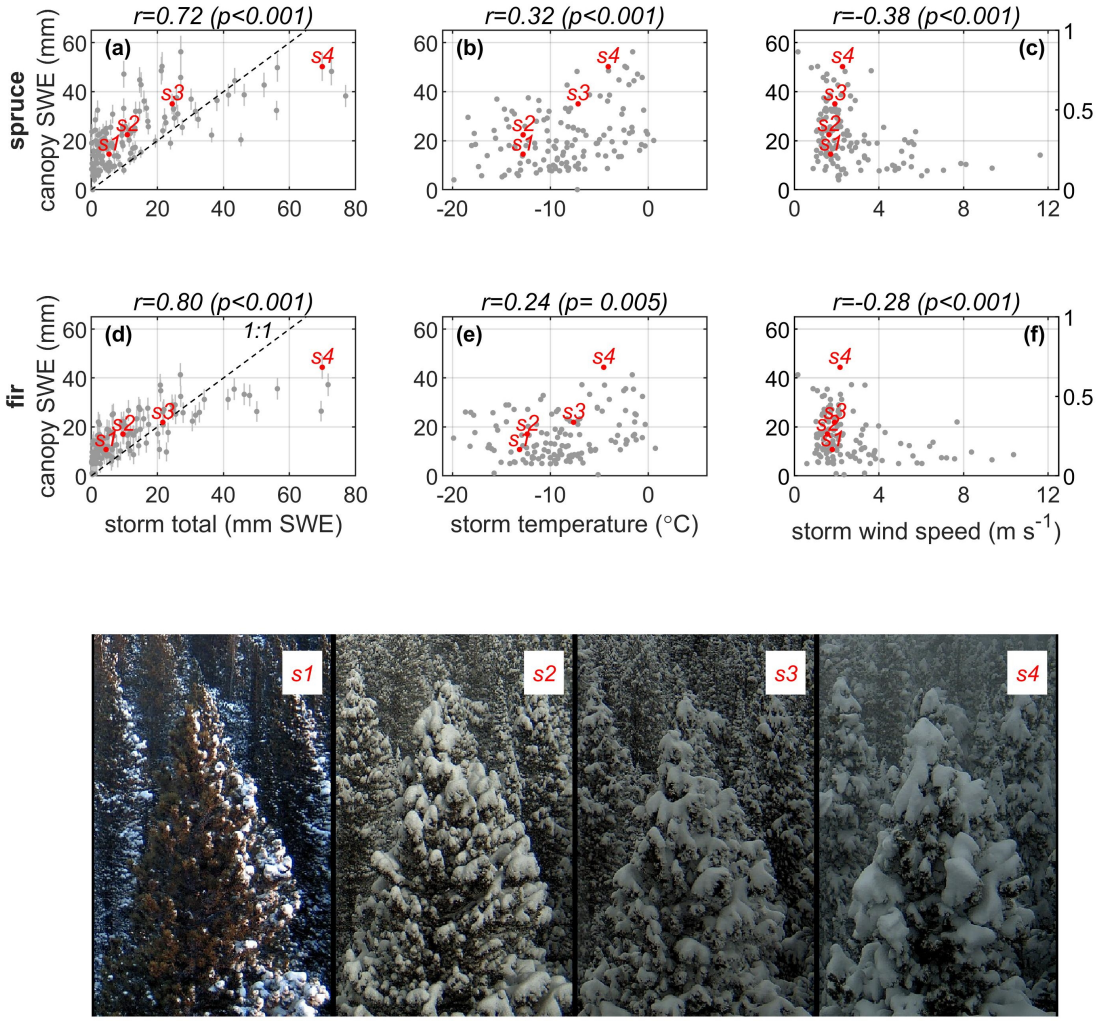

Figure 9. Sway-to-mass maximum canopy SWE of the (top row) spruce tree (n=137 storms) and (middle row) fir tree (n=136 storms) for storms over WY 2015-2020. Canopy SWE versus storm (a,d) total snowfall at the SNOTEL site, (b,e) mean wet bulb temperature, and (c,f) mean wind speed. Error bars are shown in the snowfall comparison (a,d) based on the 95% confidence interval from sway tests. Spearman's rank correlations coefficients and p-values are shown. Four storms are labeled (s1-s4) with time-lapse images shown at the bottom, with dates: 28 December 2019 (s1), 22 January 2019 (s2), 1 May 2016 (s3), and 19 May 2017 (s4).

5 Discussion

We have tested the capability for extracting quantitative snow interception in-

formation from time series of wind-induced tree sway, obtained from low-cost, non-destructive, and relatively simple installations with accelerometers. Data analysis revealed sub-daily to seasonal variations in sway frequency of two sub-alpine conifers (Figure 6), driven by intercepted snow mass and changes in tree rigidity through thaw-freeze cycles and thermal fluctuations (Figure 1). This paper has demonstrated the challenges and feasibility in disentangling these two drivers of conifer sway variations (Figures 7-8), which can permit (1) detection of snow interception and (2) quantitative estimates of canopy SWE across a range of storms (Figure 9), thereby addressing the two study questions (section 1). The six year datasets may be among the longest canopy snow records and the longest tree sway records, and are publicly available to support studies of forest ecohydrology processes (Raleigh, 2021b, 2021a).

To our knowledge, this is one of the first attempts to consider the challenges associated with applying the sway-to-mass method to measure snow intercepted in conifer canopies. The main challenges for the snow interception application are: (1) developing reliable estimates of tree sway due only to thermal effects (f_0), (2) relating changes in tree sway (Δf) to changes in mass (Δm), and (3) detecting and quantifying canopy snow during periods with low wind speeds. All challenges except for the last one may be addressed in future research that uses accelerometers; other techniques (e.g., stem compression) are necessary for measuring canopy interception in low-wind conditions. Below, we discuss these challenges.

Reliable estimates of sway variations due to thermal state (i.e., thaw-freeze cycles) can be developed with empirical relationships with temperature. When observed tree sway decreases below the range of expected thermally-driven values, snow interception can be successfully detected (Figures 7-8) with high precision scores (0.93-0.95). The model of f_0 generally showed reasonable skill (R^2 typically from 0.71 to 0.95), with improved prediction for the spruce over the fir, and similar skill when using bole temperature versus smoothed air temperature (Text S4). Prior studies have also used air temperature to estimate dynamic tree properties with comparable skill (e.g., Schmidt & Pomeroy, 1990). Improved predictions of unloaded sway might be possible by accounting for hysteresis in thaw-freeze events (Sun et al., 2019) and with more detailed models (Musselman & Pomeroy, 2017). We expect improved f_0 estimation will reduce the SNR and improve detection of more modest snow interception events (i.e., improve the recall score).

Empirical sway tests were used to convert Δf to canopy SWE (Equations 7 and 8), but this appeared to overestimate canopy SWE (see points above 1:1 line in Figure 9a,d) for multiple reasons. First, we assumed mass was concentrated in one place in the canopy (Fig. 3d), which was a simplification. Vertical distributions of canopy snow are complex and have variable center of mass with dynamic loading and unloading. If intercepted snow has a higher center of mass than the mass in our sway tests, that could cause a high bias in canopy SWE estimates. We did not characterize the canopy snow center of mass, but that might

be possible with terrestrial lidar surveys (Russell et al., 2020). Second, sway tests were only conducted under thawed conditions, and we could not assess the effect of rigidity on the conversion of Δf to canopy SWE. It is possible that the slope (i.e., dm/df) decreases with temperature; future sway tests could be completed at colder temperatures to confirm. Given our tests were at warmer conditions than many interception events, we likely overestimated canopy SWE at the coldest temperatures (i.e., highest f_0). Finally, we only tested with a modest mass (maximum near 60 kg). We extrapolated to larger snow masses, which might further contribute to errors in canopy snow estimation. As an alternative to empirical sway tests, a more mechanistic approach could yield canopy sway mass estimates by accounting for all dynamic factors influencing tree sway variations, including the height of intercepted snow, changes in biomass, variations in internal moisture content (Ciruzzi & Loheide, 2019), and variables related to tree rigidity (modulus of elasticity, DBH).

Despite these challenges, this study showed that the methodology has capabilities for improving hydrologic monitoring of snow in forested watersheds. First, the data revealed realistic changes in canopy SWE, relative to storm characteristics. Second, the data have implications for evaluating and refining modeled canopy snow processes.

We detected snow interception over a series of storms and found realistic relationships between canopy SWE and storm characteristics. Canopy SWE was significantly associated with storm SWE totals, but there were notable variations between storms (Figure 9) that were partially explained by variations in (1) wind and (2) temperature (Gutmann, 2020). Storms with high wind speeds can induce mechanical unloading and enhance sublimation; this is consistent with the observed reduction in canopy SWE with increasing wind speed, especially above 4 m s^{-1} (Fig. 9c,f). To compare, Miller (1962) suggested snow interception decreases as wind speed exceeds 2 m s^{-1}. In addition to storms with low wind, higher canopy SWE was found in storms with higher temperatures. Snow falling near the melting point is more cohesive and able to bridge conifer needles to enhance interception capacity (Kobayashi, 1987; Schmidt & Gluns, 1991). Warming temperature also reduces branch rigidity, which can induce sloughing of snow and decrease canopy SWE (Schmidt & Pomeroy, 1990). The sway-to-mass data for both trees highlight a collection of storms where the cohesion effect apparently prevails despite the potential for less rigid branches (Fig. 9b,e).

Although we do not apply process-based models, canopy SWE estimates from the sway data have potential to benefit snow and land surface model development, such as refining the representation of maximum interception and the time scales of loading and unloading. Maximum interception capacity is a common parameter in snow and land surface models (Gutmann, 2020; Rutter et al., 2009) but the parameter has noted ambiguity (Lundquist et al., 2021). The sway-to-mass estimates of canopy SWE suggest this model parameter (assuming one exists) would be at least 56 mm for the spruce, and 44 mm for the fir (Figure

9), though these may be overestimated due to limitations with the sway tests (see above). Likewise, maximum interception capacity varies with temperature in models, with two common parameterizations showing opposing temperature sensitivities, due to the processes discussed above (Lundquist et al., 2021). The canopy-to-mass data could guide selection and development of an interception parameterization that is most realistic for particular conditions.

The above interception capacity estimates are close to values found in the literature. For example, Storck et al. (2002) reported maximum interception was at least 40 mm SWE for a Douglas fir in Oregon. However, this was for a different conifer species and a different climate, highlighting the problem with data sparsity and the need for more accessible canopy SWE data in space. The 30% reduction in sway frequency of a Sitka spruce tree observed by Papesch (1984) during a snow interception event falls within the range of our values (Figure 8).

In terms of limitations, this study was confined to two coniferous trees in a continental climate, and lacked reference measurements of canopy SWE from more established techniques (e.g., weighing trees). Future work is needed for these comparisons (Klamerus-Iwan et al., 2020). The relative ease of sway measurements could enable longitudinal studies across trees (species and sizes) and climates. The sway-to-mass approach appears viable across a range of thermal states (Fig. 9b,e) and therefore may be a more universal approach than other techniques that have only worked over a limited range of climate and temperature conditions (e.g. trunk compression). However, the dependence of the sway-to-mass method on wind to activate tree motion may limit its utility in locations and times with minimal wind. Additionally, availability of existing infrastructure (e.g., an adjacent tower, Fig. 2) or the practicality and safety in tree climbing may constrain selection of trees for instrumentation.

Finally, to increase the relevance of tree sway monitoring to forested watershed modeling and management, there is a need to understand the spatial scaling of the time series data. The high correlation between our two study trees (r=0.92, Figure 6) suggests continuous sway monitoring might represent temporal variations across a forest stand. However, it is important to contextualize the sway time series observed at one or more trees relative to the sway dynamics of the greater stand. This upscaling could be achieved in multiple ways, such as mapping of sway based on allometric data (Bunce et al., 2019; T. Jackson et al., 2019; T. D. Jackson et al., 2021; Moore & Maguire, 2004; Sugden, 1962), or through resolving spatial sway variations with video-based approaches (Enuş et al., 2020). However the challenges outlined above (estimating f_0 and converting Δf to Δm) would need to be resolved at this larger scale.

6 Conclusions

Sub-daily to seasonal changes in tree sway frequency in a subalpine coniferous forest are driven by snow interception events and changes in tree thermal state with freeze-thaw cycles. By accounting for changes in tree thermal state, analysis of tree sway time series can enable detection of the timing of snow inter-

ception events and estimation of canopy SWE. In turn, these data provide novel characterization of interception dynamics between storms; such observations are rarely available.

There is a growing suite of ecohydrological processes that can be characterized by monitoring tree sway (T. D. Jackson et al., 2021); the present study has provided evidence for the application with canopy snow interception. The relative ease, cost-effectiveness (as low as $125 USD per installation), and non-destructive measurement approach of tree sway can be applied in other studies of forest processes, thereby providing new avenues for model development, which can inform resource management and environmental research. Nevertheless, several challenges need to be resolved to better constrain the sway-based estimates of canopy SWE.

Data Availability Statement

All datasets used in this study are freely available in public repositories. Raw 12 Hz tree acceleration data and hourly processed sway variables (Raleigh, 2021b, 2021a) are available for the spruce tree at https://doi.org/10.5281/zenodo.5130616 and for the fir tree at https://doi.org/10.5281/zenodo.5149308. The US-NR1 AmeriFlux data are available at https://doi.org/10.17190/AMF/1246088 and at https://doi.org/10.15485/1671825. PhenoCam imagery are available at https://PhenoCam.sr.unh.edu/. NRCS SNOTEL data are available at https://www.wcc.nrcs.usda.gov/snow/.

Acknowledgments

M. Raleigh led the study with support from the National Science Foundation (NSF EAR Award 1761441), the Advanced Study Program (ASP) at NCAR, and the CIRES Visiting Fellow program. The US-NR1 AmeriFlux site has been supported by the U.S. DOE, Office of Science through the AmeriFlux Management Project (AMP) at Lawrence Berkeley National Laboratory under Award Number 7094866. We thank Pablo Mendoza for manuscript discussions and field assistance. We also acknowledge Dan Stern, Morgan Raleigh, and Coulee Raleigh for field assistance, and Jeff Tecca for assistance with data archiving. The authors declare that they have no real or perceived conflicts of interests, financially or institutionally, in the presented work. NCAR is sponsored by the National Science Foundation. We thank the many collaborators, including site PIs and technicians, for their efforts in support of PhenoCam.

References

Baker, C. J. (1997). Measurements of the natural frequencies of trees. *Journal of Experimental Botany*, *48*(5), 1125–1132. https://doi.org/10.1093/jxb/48.5.1125Blevins, R. D. (1979). *Formulas for natural frequency and mode shape*. New York, NY: Van Nostrand Reinhold Co. https://doi.org/10.1016/0301-679x(80)90046-8Bowling, D. R., Logan, B. A., Hufkens, K., Aubrecht, D. M., Richardson, A. D., Burns, S. P., et al. (2018). Limitations to winter and spring photosynthesis of a Rocky Mountain subalpine forest. *Agricultural and Forest Meteorology*,

252, 241–255. https://doi.org/10.1016/j.agrformet.2018.01.025Bunce, A., Volin, J. C., Miller, D. R., Parent, J., & Rudnicki, M. (2019). Determinants of tree sway frequency in temperate deciduous forests of the Northeast United States. *Agricultural and Forest Meteorology*, *266–267*(December 2018), 87–96. https://doi.org/10.1016/j.agrformet.2018.11.020Burns, S. P., Blanken, P. D., Turnipseed, A. A., Hu, J., & Monson, R. K. (2015). The influence of warm-season precipitation on the diel cycle of the surface energy balance and carbon dioxide at a Colorado subalpine forest site. *Biogeosciences*, *12*(23), 7349–7377. https://doi.org/10.5194/bg-12-7349-2015Burns, S P. (2018). *The Influence of Warm-Season Precipitation on Water Cycling and the Surface Energy Budget Within and Just-Above a Colorado Subalpine Forest in Mountainous Terrain: Measurements and Modeling*. University of Colorado, Boulder.Burns, Sean P., Swenson, S. C., Wieder, W. R., Lawrence, D. M., Bonan, G. B., Knowles, J. F., & Blanken, P. D. (2018). A Comparison of the Diel Cycle of Modeled and Measured Latent Heat Flux During the Warm Season in a Colorado Subalpine Forest. *Journal of Advances in Modeling Earth Systems*, *10*(3), 617–651. https://doi.org/10.1002/2017MS001248Charrier, G., Charra-Vaskou, K., Legros, B., Améglio, T., & Mayr, S. (2014). Changes in ultrasound velocity and attenuation indicate freezing of xylem sap. *Agricultural and Forest Meteorology*, *185*, 20–25. https://doi.org/10.1016/j.agrformet.2013.10.009Charrier, G., Nolf, M., Leitinger, G., Charra-Vaskou, K., Losso, A., Tappeiner, U., et al. (2017). Monitoring of Freezing Dynamics in Trees: A Simple Phase Shift Causes Complexity. *Plant Physiology*, *173*(4), 2196–2207. https://doi.org/10.1104/pp.16.01815Church, J. (1912). The conservation of snow: its dependence on forests and mountains. *Scientific American Supplement*, *74*, 152–155.Ciruzzi, D. M., & Loheide, S. P. (2019). Monitoring Tree Sway as an Indicator of Water Stress. *Geophysical Research Letters*, *46*(21), 12021–12029. https://doi.org/10.1029/2019GL084122Dargahi, M., Newson, T., & Moore, J. R. (2020). A numerical approach to estimate natural frequency of trees with variable properties. *Forests*, *11*(9). https://doi.org/10.3390/F11090915Dickerson-Lange, S. E., Gersonde, R. F., Hubbart, J. A., Link, T. E., Nolin, A. W., Perry, G. H., et al. (2017). Snow disappearance timing is dominated by forest effects on snow accumulation in warm winter climates of the Pacific Northwest, United States. *Hydrological Processes*, *31*(10), 1846–1862. https://doi.org/10.1002/hyp.11144van Emmerik, T., Steele-Dunne, S., Hut, R., Gentine, P., Guerin, M., Oliveira, R., et al. (2017). Measuring Tree Properties and Responses Using Low-Cost Accelerometers. *Sensors*, *17*(6), 1098. https://doi.org/10.3390/s17051098van Emmerik, T., Steele-Dunne, S., Gentine, P., Oliveira, R. S., Bittencourt, P., Barros, F., & van de Giesen, N. (2018). Ideas and perspectives: Tree–atmosphere interaction responds to water-related stem variations. *Biogeosciences*, *15*(21), 6439–6449. https://doi.org/10.5194/bg-15-6439-2018Enuş, M., Dellwik, E., Mann, J., Hangan, H., & Costache, A. (2020). Three-dimensional measurements of tree crown movement using an infrared time-of-flight camera. *Experiments in Fluids*, *61*(11), 1–13. https://doi.org/10.1007/s00348-020-03053-yEssery, R., Rutter, N., Pomeroy, J., Baxter, R., Stähli, M., Gustafsson, D., et

al. (2009). SNOWMIP2: An Evaluation of Forest Snow Process Simulations. *Bulletin of the American Meteorological Society*, *90*(8), 1120–1135. https://doi.org/10.1175/2009BAMS2629.1Evans, J. R., Allen, R. M., Chung, A. I., Cochran, E. S., Guy, R., Hellweg, M., & Lawrence, J. F. (2014). Performance of Several Low-Cost Accelerometers. *Seismological Research Letters*, *85*(1), 147–158. https://doi.org/10.1785/0220130091Friesen, J., Lundquist, J., & Van Stan, J. T. (2015). Evolution of forest precipitation water storage measurement methods. *Hydrological Processes*, *29*(11), 2504–2520. https://doi.org/10.1002/hyp.10376Gao, S., Wang, X., Wang, L., & Allison, R. B. (2013). Effect of Temperature on Acoustic Evaluation of Standing Trees and Logs: Part 2: Field Investigation. *Wood and Fiber Science*, *45*(1), 15–25.Gao, S., Wang, X., & Wang, L. (2015). Modeling temperature effect on dynamic modulus of elasticity of red pine (Pinus resinosa) in frozen and non-frozen states. *Holzforschung*, *69*(2), 233–240. https://doi.org/10.1515/hf-2014-0048Gardiner, B. A. (1992). Mathematical modelling of the static and dynamic characteristics of plantation trees. In J. Franke & A. Roeder (Eds.), *Mathematical Modelling of Forest Ecosystems* (pp. 40–61). Sauerländers Verlag, Frankfurt am Main.Gerhards, C. (1982). Effect of moisture content and temperature on the mechanical properties of wood: an analysis of immediate effects. *Wood and Fiber Science*, *14*(1), 4–36.Gougherty, A. V., Keller, S. R., Kruger, A., Stylinski, C. D., Elmore, A. J., & Fitzpatrick, M. C. (2018). Estimating tree phenology from high frequency tree movement data. *Agricultural and Forest Meteorology*, *263*, 217–224. https://doi.org/10.1016/j.agrformet.2018.08.020Granucci, D., Rudnicki, M., Hiscox, A., Miller, D., & Su, H.-B. (2013). Quantifying the effects of freezing on tree sway frequencies. *Agricultural and Forest Meteorology*, *168*, 10–14. https://doi.org/10.1016/j.agrformet.2012.07.016Green, D., & Evans, J. (2008). The Immediate Effect of Temperature on the Modulus of Elasticity of Green and Dry Lumber. *Wood and Fiber Science*, *40*(3), 374–383.Green, D., Evans, J., Logan, J., & Nelson, W. (1999). Adjusting modulus of elasticity of lumber for changes in temperature. *Forest Products Journal*, *49*(10), 82–94.Guswa, A. J., Tetzlaff, D., Selker, J. S., Carlyle-Moses, D. E., Boyer, E. W., Bruen, M., et al. (2020). Advancing ecohydrology in the 21st century: A convergence of opportunities. *Ecohydrology*, *13*(4), 1–14. https://doi.org/10.1002/eco.2208Gutmann, E. D. (2020). Global modeling of precipitation partitioning by vegetation and their applications. In *Precipitation Partitioning by Vegetation: A Global Synthesis* (pp. 104–119). https://doi.org/10.1007/978-3-030-29702-2_7Gutmann, E. D., Van Stan, J. T., Friesen, J., Aubrey, D. P., & Lundquist, J. (2017). Observed compression of in situ tree stems during freezing. *Agricultural and Forest Meteorology*, *243*, 19–24. https://doi.org/10.1016/j.agrformet.2017.05.004Harpold, A. A., Guo, Q., Molotch, N., Brooks, P. D., Bales, R., Fernandez-Diaz, J. C., et al. (2014). LiDAR-derived snowpack data sets from mixed conifer forests across the Western United States. *Water Resources Research*, *50*. https://doi.org/10.1002/2013WR013935Hassinen, A., Lemettinen, M., Peltola, H., Kellomäki, S., & Gardiner, B. (1998). A prism-based system for monitoring the swaying of trees under wind loading. *Agricultural and Forest*

Meteorology, *90*(3), 187–194. https://doi.org/10.1016/S0168-1923(98)00052-5Hedstrom, N. R., & Pomeroy, J. W. (1998). Measurements and modelling of snow interception in the boreal forest. *Hydrol. Processes*, *12*, 1611–1625.Jackson, T., Shenkin, A., Moore, J., Bunce, A., van Emmerik, T., Kane, B., et al. (2019). An architectural understanding of natural sway frequencies in trees. *Journal of The Royal Society Interface*, *16*(20190116). https://doi.org/10.1098/rsif.2019.0116Jackson, T. D., Sethi, S., Dellwik, E., Angelou, N., Bunce, A., van Emmerik, T., et al. (2021). The motion of trees in the wind: a data synthesis. *Biogeosciences*, *18*(13), 4059–4072. https://doi.org/10.5194/bg-18-4059-2021Kinar, N. J., & Pomeroy, J. W. (2015). Measurement of the physical properties of the snowpack. *Reviews of Geophysics*, *53*(2), 481–544. https://doi.org/10.1002/2015RG000481Klamerus-Iwan, A., Link, T. E., Keim, R. F., & Van Stan II, J. T. (2020). Storage and Routing of Precipitation Through Canopies. In J. T. Van Stan II, E. Gutmann, & J. Friesen (Eds.), *Precipitation Partitioning by Vegetation: A Global Synthesis* (pp. 17–34). Cham: Springer International Publishing. https://doi.org/10.1007/978-3-030-29702-2_2Kobayashi, D. (1987). Snow accumulation on a narrow board. *Cold Regions Science and Technology*, *13*(3), 239–245. https://doi.org/10.1016/0165-232X(87)90005-XKooreman, B. (2013). *Measuring weight fluctuations in trees based on natural frequency*. Delft University of Technology.Lindfors, L., Atherton, J., Riikonen, A., & Hölttä, T. (2019). A mechanistic model of winter stem diameter dynamics reveals the time constant of diameter changes and the elastic modulus across tissues and species. *Agricultural and Forest Meteorology*, *272–273*, 20–29. https://doi.org/10.1016/j.agrformet.2019.03.016Lundquist, J. D., Dickerson-Lange, S. E., Lutz, J. A., & Cristea, N. C. (2013). Lower forest density enhances snow retention in regions with warmer winters: A global framework developed from plot-scale observations and modeling. *Water Resources Research*, *49*. https://doi.org/10.1002/wrcr.20504Lundquist, J. D., Dickerson-Lange, S., Gutmann, E., Jonas, T., Lumbrazo, C., & Reynolds, D. (2021). Snow interception modeling: Isolated observations have led to many land surface models lacking appropriate temperature sensitivities. *Hydrological Processes*. https://doi.org/10.1002/hyp.14274Lv, Z., & Pomeroy, J. W. (2019). Detecting intercepted snow on mountain needleleaf forest canopies using satellite remote sensing. *Remote Sensing of Environment*, *231*(111222), 1–19. https://doi.org/10.1016/j.rse.2019.111222Lv, Z., & Pomeroy, J. W. (2020). Assimilating snow observations to snow interception process simulations. *Hydrological Processes*, 1–18. https://doi.org/10.1002/hyp.13720Martin, K. A., Van Stan, J. T., Dickerson-Lange, S. E., Lutz, J. A., Berman, J. W., Gersonde, R., & Lundquist, J. D. (2013). Development and testing of a snow interceptometer to quantify canopy water storage and interception processes in the rain/snow transition zone of the North Cascades, Washington, USA. *Water Resources Research*, *49*. https://doi.org/10.1002/wrcr.20271Mayhead, G. J. (1973). Sway periods of forest trees. *Scottish Forestry*, *27*(1), 19–23.Miller, D. H. (1962). Snow in the trees – where does it go? In *Proc. 30th Western Snow Conference* (pp. 21–27). Cheyenne.Moeser, D., Mazzotti, G.,

Helbig, N., & Jonas, T. (2016). Representing spatial variability of forest snow: Implementation of a new interception model. *Water Resources Research*, *52*. https://doi.org/10.1002/2015WR017961Molotch, N. P., Blanken, P. D., Williams, M. W., Turnipseed, A. A., Monson, R. K., & Margulis, S. A. (2007). Estimating sublimation of intercepted and sub-canopy snow using eddy covariance systems. *Hydrological Processes*, *21*(12), 1567–1575. https://doi.org/10.1002/hyp.6719Montesi, J., Elder, K., Schmidt, R. A., & Davis, R. E. (2004). Sublimation of Intercepted Snow within a Subalpine Forest Canopy at Two Elevations. *Journal of Hydrometeorology*, *5*(5), 763–773. https://doi.org/10.1175/1525-7541(2004)005<0763:SOISWA>2.0.CO;2Moore, J. R., & Maguire, D. A. (2004). Natural sway frequencies and damping ratios of trees: concepts, review and synthesis of previous studies. *Trees - Structure and Function*, *18*(2), 195–203. https://doi.org/10.1007/s00468-003-0295-6Musselman, K. N., & Pomeroy, J. W. (2017). Estimation of Needleleaf Canopy and Trunk Temperatures and Longwave Contribution to Melting Snow. *Journal of Hydrometeorology*, *18*(2), 555–572. https://doi.org/10.1175/JHM-D-16-0111.1Musselman, K. N., Molotch, N. P., & Brooks, P. D. (2008). Effects of vegetation on snow accumulation and ablation in a mid-latitude sub-alpine forest. *Hydrological Processes*, *22*(15), 2767–2776. https://doi.org/10.1002/hyp.7050Nakai, Y., Sakamoto, T., Terajima, T., Kitahara, H., & Saito, T. (1994). Snow interception by forest canopies: weighing a conifer tree, meteorological observation and analysis by the Penman-Monteith formula. In *Snow and Ice Covers: Interactions with the Atmosphere Ecosystems, IAHS Publ. no. 223* (pp. 227–236).Onwona-Agyeman, S., Morioka, N., Kondo, M., & Kitagawa, K. (1995). Seasonal changes in the Modulus of Elasticity of living branches of three coniferous species. *Ecological Research*, *10*(2), 199–206. https://doi.org/10.1007/BF02347942Papesch, A. J. . (1984). *Wind and its effects on (Canterbury) forests. University of Canterbury.* University of Canterbury.Peltola, H. (1996). Swaying of trees in response to wind and thinning in a stand of Scots pine. *Boundary-Layer Meteorology*, *77*(3–4), 285–304. https://doi.org/10.1007/BF00123529Pivato, D., Dupont, S., & Brunet, Y. (2014). A simple tree swaying model for forest motion in windstorm conditions. *Trees - Structure and Function*, *28*, 281–293. https://doi.org/10.1007/s00468-013-0948-zPomeroy, J.W., & Dion, K. (1996). Winter radiation extinction and reflection in a boreal pine canopy: measurements and modelling. *Hydrological Processes*, *10*(12), 1591–1608. https://doi.org/10.1002/(SICI)1099-1085(199612)10:12<1591::AID-HYP503>3.0.CO;2-8Pomeroy, John W., & Schmidt, R. A. (1993). The use of fractal geometry in modelling intercepted snow accumulation and sublimation. In *Proc. 50th Eastern Snow Conference* (pp. 1–10). Quebec City.Raleigh, M. S. (2021a). Multi-year measurements of tree motion from an accelerometer on a fir tree near Niwot Ridge, Colorado. https://doi.org/10.5281/zenodo.5149308Raleigh, M. S. (2021b). Multi-year measurements of tree motion from an accelerometer on a spruce tree near Niwot Ridge, Colorado. https://doi.org/10.5281/zenodo.5130616Raleigh, M. S., Rittger, K., Moore, C. E., Henn, B., Lutz, J. A., & Lundquist, J. D. (2013). Ground-based testing of MODIS fractional snow cover in subalpine meadows

and forests of the Sierra Nevada. *Remote Sensing of Environment*, *128*, 44–57. https://doi.org/10.1016/j.rse.2012.09.016Richardson, A. D., Hufkens, K., Milliman, T., Aubrecht, D. M., Chen, M., Gray, J. M., et al. (2018). Tracking vegetation phenology across diverse North American biomes using PhenoCam imagery. *Scientific Data*, *5*, 180028. https://doi.org/10.1038/sdata.2018.28Roth, T. R., & Nolin, A. W. (2019). Characterizing Maritime Snow Canopy Interception in Forested Mountains. *Water Resources Research*, *55*(6), 4564–4581. https://doi.org/10.1029/2018WR024089Russell, M., U. H. Eitel, J., J. Maguire, A., & E. Link, T. (2020). Toward a Novel Laser-Based Approach for Estimating Snow Interception. *Remote Sensing*, *12*(7), 1146. https://doi.org/10.3390/rs12071146Rutter, N., Essery, R., Pomeroy, J., Altimir, N., Andreadis, K., Baker, I., et al. (2009). Evaluation of forest snow processes models (SnowMIP2). *Journal of Geophysical Research*, *114*, 1–18. https://doi.org/10.1029/2008JD011063Schmidt, R. A., & Gluns, D. R. (1991). Snowfall interception on branches of three conifer species. *Canadian Journal of Forest Research*, *21*(8), 1262–1269. https://doi.org/10.1139/x91-176Schmidt, R. A., & Pomeroy, J. W. (1990). Bending of a conifer branch at subfreezing temperatures: implications for snow interception. *Canadian Journal of Forest Research*, *20*(8), 1251–1253. https://doi.org/10.1139/x90-165Selker, J. S., Lane, J. W., Rupp, D. E., Hut, R., Abou Najm, M. R., Stewart, R. D., et al. (2011). The answer is blowing in the wind: using wind induced resonance of trees to measure time varying canopy mass, including interception. In *AGU Fall Meeting*. #H11G-1155.Silins, U., Lieffers, V. J., & Bach, L. (2000). The effect of temperature on mechanical properties of standing lodgepole pine trees. *Trees*, *14*(8), 424–428. https://doi.org/10.1007/s004680000065Van Stan, J. T., Martin, K. A., Friesen, J., Jarvis, M. T., Lundquist, J. D., & Levia, D. F. (2013). Evaluation of an instrumental method to reduce error in canopy water storage estimates via mechanical displacement. *Water Resources Research*, *49*(1), 54–63. https://doi.org/10.1029/2012WR012666Storck, P., Lettenmaier, D., & Bolton, S. (2002). Measurement of snow interception and canopy effects on snow accumulation and melt in a mountainous maritime climate, Oregon, United States. *Water Resources Research*, *38*(11), 1–16.Sugden, M. J. (1962). Tree sway period - a possible new parameter for crown classification and stand competition. *The Forestry Chronicle*, *38*(3), 336–344. https://doi.org/10.5558/tfc38336-3Sun, Y., Zhou, H., Shan, G., Grantz, D. A., Schulze Lammers, P., Xue, X., et al. (2019). Diurnal and seasonal transitions of water and ice content in apple stems: Field tracking the radial location of the freezing- and thawing-fronts using a noninvasive smart sensor. *Agricultural and Forest Meteorology*, *274*(February), 75–84. https://doi.org/10.1016/j.agrformet.2019.04.018Turnipseed, A. A., Blanken, P. D., Anderson, D. E., & Monson, R. K. (2002). Energy budget above a high-elevation subalpine forest in complex topography. *Agricultural and Forest Meteorology*, *110*(3), 177–201. https://doi.org/10.1016/S0168-1923(01)00290-8USDA Forest Service. (2010). *Wood Handbook*. (R. J. Ross, Ed.), *General Technical Report FPL-GTR-190*. Madison: USDA Forest Service Forest Products Laboratory.Varhola, A., Coops, N. C., Weiler, M., & Moore, R. D. (2010). Forest canopy effects on snow accumulation and ablation: An

integrative review of empirical results. *Journal of Hydrology*, *392*(3–4), 219–233. https://doi.org/10.1016/j.jhydrol.2010.08.009Yang, Z., Hui, K. W., Abbas, S., Zhu, R., Kwok, C. Y. T., Heo, J., et al. (2021). A Review of Dynamic Tree Behaviors: Measurement Methods on Tree Sway, Tree Tilt, and Root–Plate Movement. *Forests*, *12*(3), 379. https://doi.org/10.3390/f12030379